Journal of Materials Chemistry A

Accepted Manuscript

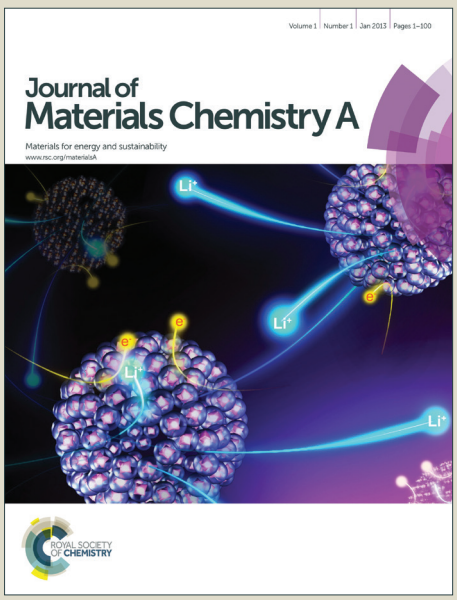

ROYAL SOCIETY OF CHEMISTRY

www.rsc.org/materialsA

Cite this: DOI: 10.1039/c0xx00000x

www.rsc.org/xxxxxx

ARTICLE TYPE

Self-aligned graphene as anticorrosive barrier in waterborne polyurethane composite coatings

Yaya Li[a], Zhenzhen Yang[a], Hanxun Qiu[a], Yigang Dai[b], Qingbin Zheng[a], Jing Li[a*] and Junhe Yang[a*]

Received (in XXX, XXX) Xth XXXXXXXXX 20XX, Accepted Xth XXXXXXXXX 20XX

DOI: 10.1039/b000000x

Graphene reinforced waterborne polyurethane (PU) composite coatings were fabricated on steel surfaces. Self-alignment of graphene was driven, when the filler content was 0.4 wt%, by the reduction of the total excluded volume. The superior anticorrosion properties were proven by Electrochemical Impedance Spectrum (EIS) analysis for the PU matrix composite coating reinforced by 0.4 wt% of aligned graphene. The interaction mechanism between electrolyte and graphene layers was discussed for the three-dimensional randomly distributed graphene and the in-plane aligned graphene, respectively, to better understand their effects as the anticorrosive barriers.

1. Introduction

Graphene, a two-dimensional graphitic carbon material, has unique geometry and novel physical properties, like high aspect ratio, electrical and thermal conductivity and barrier properties. Those interesting properties intrigued the research excitement on the applications of graphene in anticorrosive coatings.[1-4]

Dhiraj Prasai et al. reported that graphene film fabricated by chemical vapor deposition can act as an efficient anticorrosive coating on the surface of copper.[1] The graphene films worked as a barrier to molecules such as O_2 and H_2O, although the long-term anticorrosion properties of the graphene film were decayed, due to the large number of defects of the graphene film grown by chemical vapor deposition method.[2] Another efficient way to benefit from the barrier properties of graphene was to incorporate the reduced graphene oxide (rGO) in a polymer matrix to produce composite materials.[5-8] Thereafter, the composite materials with enhanced barrier properties can be applied as an organic coating on metal surfaces. It has been shown that the anticorrosion properties of the functionalized-graphene reinforced polymer composite coatings were improved, owning to the enhanced barrier properties by graphene additives.[3, 4]

Similar studies have been reported on nano-clay reinforced polyaniline composites and their coatings on steel surfaces. The free-standing composite film exhibited a 400% reduction in O_2 permeability compared to conventional polyaniline, which in turn offered significantly enhanced corrosion protection in the form of composite coatings.[9] Theoretical model has been developed based on the simple tortuosity-based approach and renormalization group theory to quantitatively evaluate the geometric factors, such as aspect ratio, orientation of clay platelets on barrier properties of clay/polymer nanocomposites.[10] The theoretical predictions showed that high aspect ratio and in-plane alignment further enhanced the barrier properties perpendicular to the alignment. Graphene, with thickness around 1 nm and diameter ranging from several microns to several hundred microns, tended to have higher aspect ratio than nano-clay. Experimental studies proved that graphene reinforced polymer composites had lower gas permeability than clay reinforced polymer composites with same loading ratio.[3,5] In addition to the aspect ratio and the in-plane alignment, the dispersion of graphene in a polymeric matrix was another important factor on the properties of composites and their coatings.[11, 12]

In this paper, we fabricated anticorrosive composite coatings on electro galvanized steel (EG) surfaces with waterborne PU as the organic matrix and functionalized rGO with high aspect ratio as the reinforcement. To avoid the agglomeration of rGO, graphene oxide (GO) was treated by the method reported in our previous publication on microwave assisted reduction and titanate functionalization of GO.[13] Superior anticorrosion properties of the composite coatings were obtained by adding 0.4 wt% high aspect ratio, aligned graphene.

[a]*School of Materials Science and Engineering, University of Shanghai for Science and Technology, No.516 Jungong Road, Shanghai 200093, China*

[b]*Research Institute, Baoshan Iron & Steel Co. ltd., No. 889 Fujin Road, Shanghai 201900, China*

Corresponding author: Tel)+86-21-55271689; Fax) +86-21-55270632; E-mail: lijing6080@usst.edu.cn

Tel) +86-21-55274065; Fax) +86-21-55270632; E-mail: jhyang@usst.edu.cn

2. Experimental

2.1 Reduction and functionalization of GO

GO, prepared by modified Hummers method[14], was reduced and functionalized simultaneously with microwave-assistance, as described in our previous paper.[13] Typically, 100 ml GO/DI water solution (1 mg ml^{-1}) was mixed with 5ml hydrazine hydrate (85%) and 0.5 g titanate coupling agent (TM-200S, Yangzhou Tianyang Auxiliaries Co. Ltd.). The mixture was treated while stirring using a microwave reactor (CEM, Discover SP) at 120°C for 10 min, followed by filtration and flush with DI water repeatedly to eliminate the unreacted titanate coupling agent and hydrazine hydrate. The product, referred as TGO, was diluted in DI water (1 mg ml^{-1}) and sonicated for 10 min in a bath sonicator. The solution can be held stable for months, owning to the covalently bonded titanate coupling agent. The thickness of TGO was around 1nm, according to the estimation based on high resolution TEM image, as published previously.[13]

2.2 Preparation of the TGO/PU composite coatings

The aqueous solution of TGO was mixed with waterborne PU (NeoRez R-9679, DSM, the solid content is 37 wt%). A certain amount of DI water was added to obtain a solid content of 20 wt%. The mixture was stirred magnetically for 30min. EG sheets (80mm*40mm*1mm), supplied by Baosteel Ltd. (Shanghai), were thoroughly cleaned by sonication in alkaline degreaser (Henckle, Shanghai) for 10 min, flushing using DI water and sonication in ethanol for another 10min. The liquid composite coatings were applied on the EG surfaces with a bar coater, and then the specimens were baked in a vacuum oven at 110℃ for 30 min. Coated samples were referred as PU, PTG-0.2 and PTG-0.4, according to the wt% of TGO in the solid content of composite coatings (0%, 0.2% and 0.4% respectively).

2.3 Characterizations

A transmission electron microscope (TEM, FEI Tecnai G2 SpiritBiotwin) was used to evaluate the nanoscopic dispersion state of TGO in PU matrix at an acceleration voltage of 120 kV. For TEM sample preparation, a free-standing TGO/PU composite thin film was moulded on a Teflon surface and dried at 50°C for 24 h in a vacuum oven. The composite thin film was embedded in an epoxy matrix and microtomed (Leica UC6) into 100 nm thick slices with a diamond knife. A 400 mesh copper grid was used to collect the ultra-thin TEM samples. In order to identify the microscopic distribution of TGO in the composite coatings, the cryogenic fracture surfaces of the coated EG sheets were examined using a scanning electron microscope (SEM, Quanta FEG450 FEI Co., Ltd, USA).

For the Electrochemical Impedance Spectroscopy (EIS), a three-electrode cell was used: the coated EG surface as the working electrode with an exposed area of 1cm^2, the saturated Ag/AgCl (0.205V vs. SHE) as the reference electrode and a platinum counter electrode. The electrolyte was a 3.5 wt% NaCl solution (reagent grade). Electrochemistry workstation (PARSTAT 4000, Princeton Applied Research) was employed with the low current interface attachment. The signal amplitude was 5 mV relative to the open circuit potential and the frequency was ranged from 0.1 to 10000 Hz. All the EIS measurements were performed in a Faraday cage at room temperature and repeated three times in order to verify the accuracy and repeatability of the measurements. EIS data were analyzed by Zview 2.70 software.

The salt spray test was carried out on coated EG plates (40mm×80mm) with a 5% NaCl solution at 100% relative humidity at 35 °C according to ASTM B117-03. The samples were checked every 12 h and images were recorded to validate the EIS results.

3. Results and discussions

3.1 Morphologies of the TGO/PU composites and their coatings

SEM micrographs taken from fracture surfaces of PU, PTG-0.2 and PTG-0.4 were shown in Fig. 1. The thickness of the coatings can be estimated to be around 15 um from the low magnification images, Fig. 1a and b. Neat PU coating exhibited relatively smooth fracture surfaces, as shown in Fig. 1a and a'. A random distribution of TGO was shown in PTG-0.2, as in Fig. 1b'. With the TGO content increased to 0.4 wt%, the fracture surface of PTG-0.4 became relatively rough as in Fig. 1c, due to the distribution of TGO. Moreover, TGO showed a two-dimensional alignment parallel to the EG substrate (Fig. 1c'), which tended to provide the EG substrate enhanced barrier protection.[10] The self-alignment of platelet-shaped nano-fillers in polymer composite films has been observed for clay/Nafion,[15] rGO/PU,[8,16] GO/Nafion and rGO/Nafion[17] composite films. In these cases, the spontaneous alignment of the platelet-shaped nano-fillers usually involved the volume shrinks (e.g., due to solvent evaporation). The main driving force of the self-alignment is the entropic gain associated with reducing the total excluded volume.[18]The total excluded volume of non-spherical rigid particles depends on the aspect ratio, the orientation and the concentration of the particles.[19,20] High aspect ratio and high concentration of the particles increase the total excluded volume, while the tendency of reduction of the total excluded volume drives the particles to align spontaneously. Therefore, the high aspect ratio and a 0.4 wt% concentration of TGO were crucial for its self-alignment. Besides, there were some conditional parameters which were expected to promote the self-alignment of TGO, including the low viscosity of the wet-painting, the controlled evaporation rate of the solvent and the elevated temperature during the film formation.

The TEM images in Fig. 2 showed the nanoscopic dispersion state of TGO in moulded TGO/PU composite thin films. The dark lines represented individual graphene layers, while the bright area represented the PU matrix. TGO was well dispersed in PU matrix at low concentration of 0.05 wt% as shown in Fig. 2a, because the compatibility between TGO and the PU chain was improved by the titanate functionalization. The curvature of TGO platelets can be revealed by TEM, compared to the flat platelets observed in SEM images. In Fig. 2b, the dark area represented the agglomerated TGO in nanoscopic localized area, indicating the localized dispersion of TGO was deteriorated to some extent at higher concentration of 0.4 wt% of TGO, driven by the reduction of surface free energy. It was interesting to note that the

nanoscopic agglomeration and the microscopic self-alignment of TGO were observed at the same filler content of 0.4 wt%. A plausible explanation was that the interparticle distances decreased with increasing the TGO content, so the strong interaction between the adjacent TGO particles favored their rotation and diffusion during the solvent evaporation and the system was allowed to lower its free energy by forming alignment and agglomeration.

3.2 Anticorrosion properties of the TGO/PU coatings

Fig. 3 showed the EIS spectra of PU, PTG-0.2 and PTG-0.4 coatings with different exposure durations. The Bode phase plot, Bode modulus plot and Nyquist plot of PU coatings were in Fig. 3a, a' and a''. For an intact coating without defects, the phase angle in Bode plot should be 90 degree due to the pure resistance characteristics of the coating. As the electrolyte solution gradually permeated into the coating, the phase angle at a given

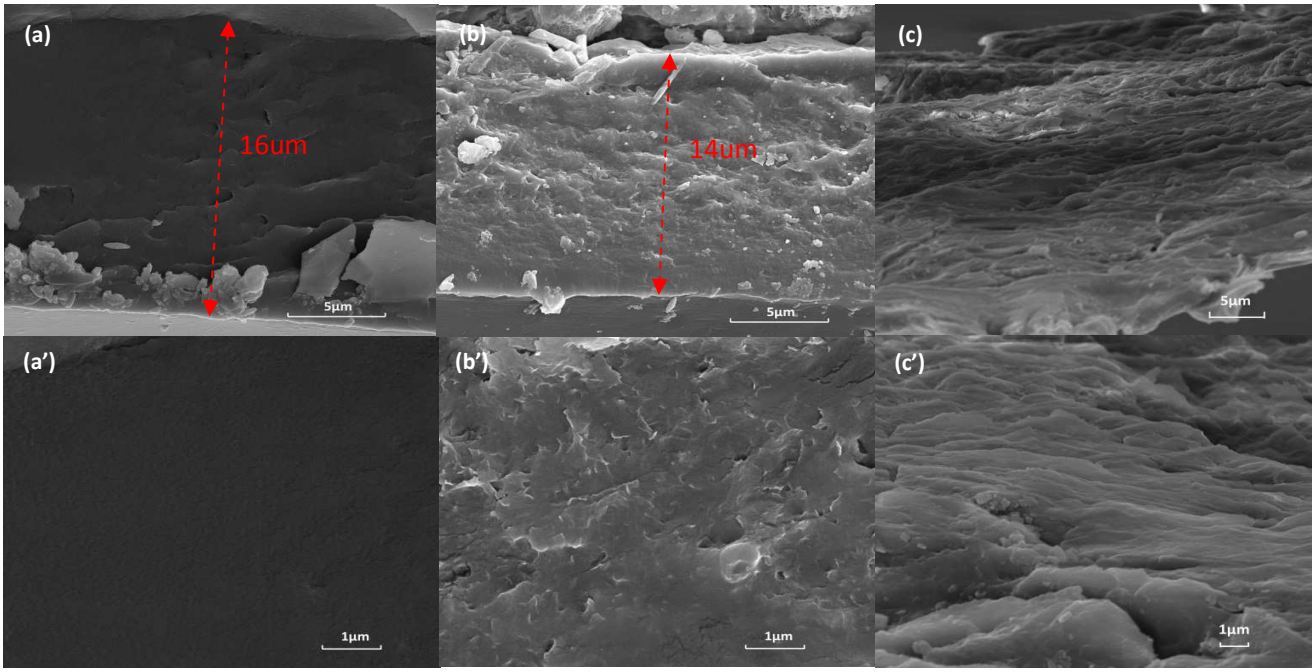

Fig. 1 SEM micrographs of fractured surfaces of the coatings: (a)(a')PU,(b)(b')PTG-0.2 and (c)(c')PTG-0.4.

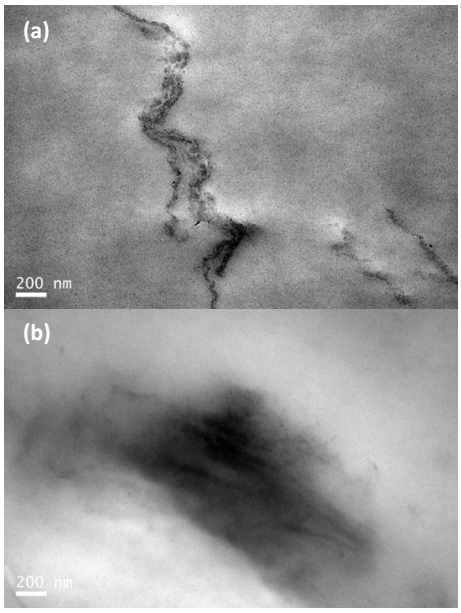

Fig. 2 TEM micrographs of the TGO/PU nanocomposites containing (a) 0.05 wt% and (b) 0.4 wt% of TGO.

frequency decreased due to the parallel capacitance characteristics of the coating. The variations of phase angles may reflect the performance of coatings.[21] The peak at different frequency range in the Bode phase plot represented for different time constant. The time constant appeared at high frequency range can be attributed to the coating layer, while the time constant at low frequency range was corresponding to a corrosion process taking place at the metal/coating interface.[22] The phase angle plot showed two time constants at very beginning of the immersion of 1h. With increasing the immersion duration, the phase angle decreased dramatically and the time constant at low frequency range gradually disappeared, revealing that the barrier properties of the coating were deteriorated quickly and large area of delaminating occurred at the metal/coating interface due to the corrosion reaction, which was modelled as stage III of corrosion process. The impedance modulus at 0.1 Hz, which represented the ability of the coating to impede the flow of current between anodic and cathodic areas, decreased two orders of magnitudes after 100h immersion. In Nyquist plot, the tremendous decrease of the radius also confirmed the rapid drop of the efficacy of PU coating. At the immersion duration of 1h and 4h, the inverse trend of increased impedance at low frequency range and radius in Nyquist plot was observed, which was probably due to the quick penetration of the electrolytes and the formation of the

transient passivation layer of the corrosion product.

The Bode plots and Nyquist plot of PTG-0.2 coating were presented in Fig. 3b, b' and b'' with varying immersion durations. One time constant and peak phase angle of near-90° demonstrated the capacitance nature of the coating at 1h immersion, which was defined as stage I of the corrosion process. After immersion of 4h, a second time constant can be observed by Nyquist plot, although it was not clearly shown in phase angle plot, which was corresponding to the initiation of the under-painting corrosion. Stage II of the corrosion process started at this point. With increasing the immersion duration to 96h, stage II corrosion process with two time constants kept going. In the phase angle plot, the peaks at high frequency range weakened continuously, indicating the penetration of the electrolyte in the coatings. The impedance modulus at 0.1Hz was decreased for about 1 order of magnitude, from $4x10^7$ Ω to $5x10^6$Ω. Stage III corrosion was not observed for PTG-0.2 coating. With the addition of 0.2 wt% TGO, three-dimensional randomly distributed, the anticorrosion properties of the coating has been significantly improved, compared to neat PU coating.

Fig. 3c, c' and c'' presented the EIS results for PTG-0.4 coatings. One time constant at high frequency range was appreciated throughout the 96h immersion duration, as shown in the Bode phase plot and the Nyquist plot. Although there was gradual decrease of phase angle and impedance modulus at 0.1Hz, the stage I corrosion process was maintained for 96h of immersion. The most substantial improvement of anticorrosion properties was achieved by 0.4 wt% self-aligned TGO, which functioned as multi-layer barriers to the environmental attacking.

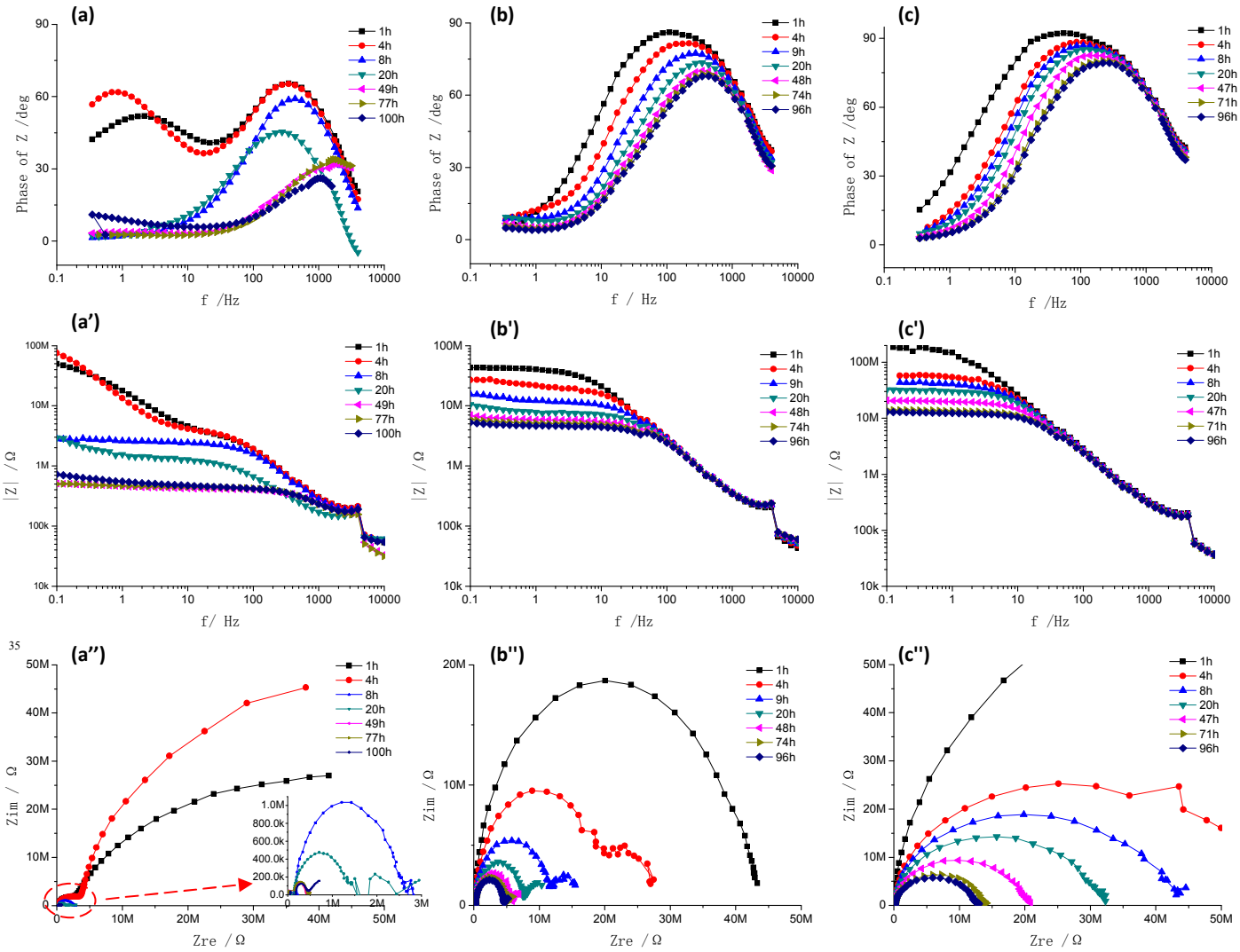

Fig. 3 EIS spectra of the three coating with different immersion durations: (a),(a'),(a'') are the Bode Phase plot, Bode modulus plot, Nyquist plot of neat PU coating; (b),(b')(b'') are the Bode Phase plot, Bode modulus plot, Nyquist plot of the PTG-0.2 coating; (c),(c'),(c'') are the Bode Phase plot, Bode modulus plot, Nyquist plot of the PTG-0.4 coating.

Breakpoint frequency (f_b) was employed to analyze the delaminated area of organic coatings.[22,23] This approach was based on the breakpoint method discussed by Haruyama et al., which used high-frequency data to obtain the electrochemically active area.[24] The f_b was defined as the frequency corresponding to a 45°-phase angle at high frequency range. The porosity of the

coating surfaces and the reaction at the metal/coating interface could be analyzed by the variation of f_b with immersion durations. Their relations were presented as $f_b = K (A_t/A_0)$, Where A_t was the delaminated area, A_0 was the total area of the sample, $K = (1/2)\rho\varepsilon\varepsilon_0$, ρ was the resistivity of the coating, ε was the dielectric constant of electrolyte in the coating, and ε_0 was the vacuum permittivity.[25] With the electrolyte solution penetrated through the organic coating, the value of ρ declined, while the value of ε increased accordingly. The compensation effect made it possible that K could be approximately seen as a constant, given ε_0 was a constant. Therefore, the delaminated area of the coating was approximately proportional to f_b.[23]The value of f_b for the three coatings was plotted against immersion durations in Fig. 4. The f_b of the PU coatings increased dramatically with the immersion duration, the f_b of PTG-0.2 increased intermediately, while the f_b of PTG-0.4 had a marginal increase. It was evident that the anticorrosion properties of the coatings improved significantly with increasing the TGO content.

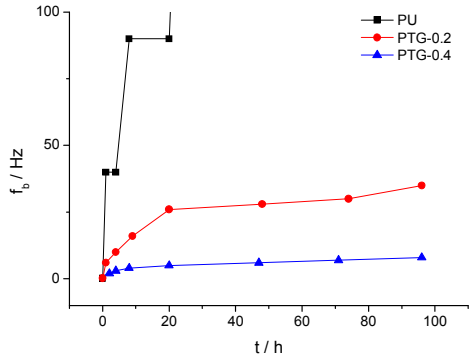

Fig. 4 The breakpoint frequency f_b as a function of immersion duration for PU, PTG-0.2 and PTG-0.4 coatings.

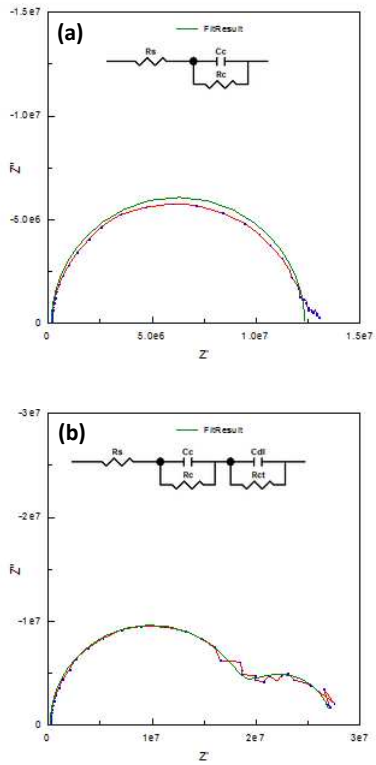

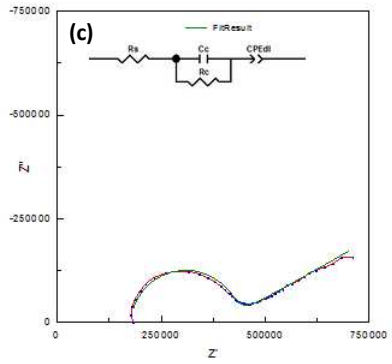

Fig. 5 Comparison of experimental data and fitting curves, with the corresponding equivalent circuits inserted. (a)Stage I (PTG-0.4 coating at 96h) (b) Stage II (PTG-0.2 coating at 4h) (c) Stage III (PU coating at 100h).

The equivalent circuits for stage I, stage II, and stage III corrosion process were used to fit the Nyquist plots of EIS results. The typical fitting curves and the corresponding equivalent circuits were shown in Fig. 5 for different corrosion stages. In the equivalent circuits, Rs was the resistance of solution, Rc was the resistance of coating, Cc was the double electrode layer capacitance of coating, Rct was the charge transfer resistance of corrosion electrochemical reaction in the metal/coating interface, Cdl was the double electrode layer capacitance in the interface, the constant phase angle element CPEdl was the calibration of Cdl deviating from ideal double electrode layer.[26,27] The typical curves in Fig. 5 showed a good agreement between the fitting curves and the experiment data. Two of the deviation parameters, chi-sqr and sum-sqr, were calculated to indicate the accuracy of the fitting. The fitting results were listed in Tab. 1 for PU, PTG-0.2 and PTG-0.4 coatings. The neat PU coating went to stage II of corrosion at 1h of immersion, and changed to the stage III at 77h. The PTG-0.2 coating was in stage I at 1h and kept in stage II from 4h to 96h. The PTG-0.4 coating stayed in stage I for 96h.

The values of electrochemical parameters Rc and Cc were obtained from the fitting and plotted in Fig. 6 against the immersion durations. As the electrolyte solution penetrated through the coatings, the coating resistance Rc would decrease.[22] As shown in Fig. 6a, the protective performance of PU coating degraded more quickly than the other two coatings. The PTG-0.4 coating exhibited the best anti-penetration of the electrolyte solution, which was consistent with the Stage I corrosion throughout the immersion duration. Cc would increase with the absorption of the electrolyte solution in the coating. As in Fig. 6b, the PU coating showed the most remarkable increase of Cc and the Cc value after electrolyte exposure was about 1 order of magnitude higher than the other two coatings. The Cc of PTG-0.4 coating was marginally higher than PTG-0.2 coating, although they were in the same order of magnitude, which indicated PTG-0.4 coating absorbed a little more electrolyte than PTG-0.2. The reasons could be that the interaction mechanism between electrolyte and TGO was different for the coatings with randomly distributed TGO and aligned TGO, in addition to the different TGO contents. The TGO layers acted barriers for the diffusion of small molecules. Randomly distributed TGO layers could seal up

some localized area in the coating, which limited the absorption of electrolyte, while in-plane aligned TGO offered more opportunities for the electrolyte to interact with the TGO layers, leading to a full utilization of the high surface area offered by the TGO layers.[28]

Tab. 1 Fitting results for (a)PU, (b) PTG-0.2 and (c) PTG-0.4 coatings.

(a)

Time/h	1	4	49	77
Stage	II	II	II	III
Chi-sqr	0.0043	0.0069	0.0031	0.0008
Sum-sqr	0.38	0.62	0.27	0.06
Rs /Ω	1.88E+05	2.05E+05	1.47E+05	94993
Cc /F	8.10E-10	7.80E-10	1.04E-09	1.16E-09
Rc /Ω	2.01E+06	3.53E+06	2.70E+05	2.72E+05
Cdl /F	8.74E-09	1.30E-08	1.84E-06	\
Rct /Ω	7.53E+07	9.05E+07	80704	\
CPEdl-T /F	\	\	\	7.63E-06
CPRdl-P /F	\	\	\	0.12

(b)

Time/h	1	4	48	74
Stage	I	II	II	II
Chi-sqr	0.0106	0.0028	0.0038	0.0033
Sum-sqr	0.95	0.25	0.33	0.30
Rs /Ω	1.83E+05	1.98E+05	2.14E+05	2.12E+05
Cc /F	5.70E-10	5.33E-10	5.54E-10	5.62E-10
Rc /Ω	4.07E+07	1.87E+07	5.50E+06	4.81E+06
Cdl /F	\	3.39E-08	6.02E-07	8.01E-07
Rct /Ω	\	8.33E+06	1.84E+06	1.32E+06

(c)

Time/h	1	4	47	71
Stage	I	I	I	I
Chi-sqr	0.0145	0.0102	0.0071	0.0073
Sum-sqr	1.26	0.89	0.65	0.66
Rs /Ω	1.73E+05	1.71E+05	1.63E+05	1.58E+05
Cc /F	5.65E-10	5.81E-10	6.19E-10	6.46E-10
Rc /Ω	1.72E+08	5.53E+07	1.98E+07	1.34E+07

Images of the coated EG samples after the salt spray test were shown in Fig. 7. Large area of white corrosion product appeared after 48h exposure for the neat PU coated EG plates. For the EG plates coated with TGO/PU composite coatings, no corrosion product was observed, although there were some blisters, indicating that the TGO/PU composite coatings had better anticorrosion properties. The salt spray test is widely used in industrial, but the precision is not comparable with EIS test. The difference of corrosion resistance between PTG-0.2 coating and PTG-0.4 coating was hard to identify.

A schematic drawing in Fig. 8 showed the interaction mechanism between electrolyte and TGO layers with different distributions in the PU-matrix coatings. Fig. 8a presented a three-dimensional randomly distributed TGO, as the case of PTG-0.2 coating, which gave a tortuous path of electrolyte to penetrate through the coating[10,29]. The anticorrosion properties could be improved because it took longer time for electrolyte to penetrate through the coating and reach the metal/coating interface along the tortuous path. Besides, when the filler content was high enough to form some barrier networks in the coating, some portions of the coating were sealed up, which gave lower absorption of the electrolyte. For composite coating with in-plane aligned TGO, Fig. 8b showed an interaction mechanism which fully utilized the surface area of TGO as the barrier to prevent the electrolyte from penetration through the coating. To benefit from the multilayer anticorrosive barriers offered by TGO, it was important to have a good nanoscopic dispersion of TGO, in addition to its in-plane alignment and high aspect ratio. In our experiment, the titanate functionalization was employed to avoid the agglomeration of TGO. PTG-0.4 coating remained stage I corrosion process for 96h, which indicated the electrolyte did not penetrate to the metal/coating interface. The reason of the superior anticorrosion properties of PTG-0.4 coating included 1) relatively high TGO content, 2) In-palne alignment, 3) high aspect ratio and 4) acceptable nanoscopic dispersion of TGO.

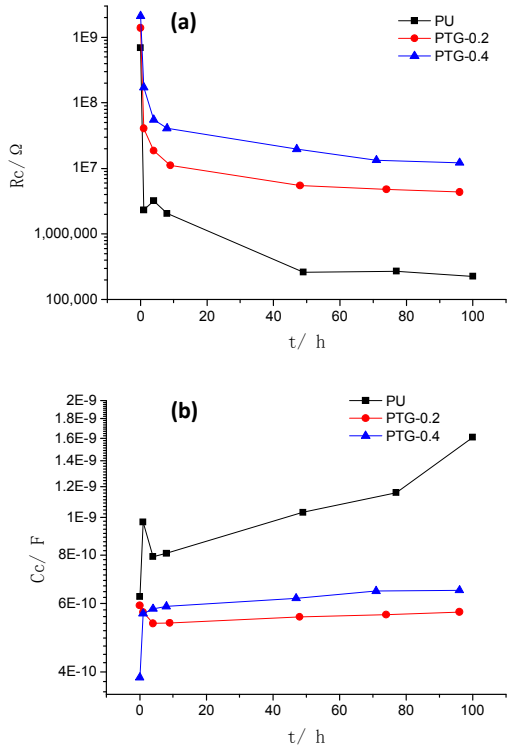

Fig. 6 Evolution of (a) Rc and (b) Cc of the three coatings.

Conclusion

Graphene reinforced waterborne PU composite coatings were fabricated on steel surfaces. Titanate functionalization of graphene was employed to facilitate the dispersion of graphene in the composite coatings. The morphologies and anticorrosion properties of the composite coatings were characterized. When the graphene content was 0.2 wt%, three-dimensional random distribution of graphene was observed in the composite coatings, which gave a tortuous path of electrolyte to penetrate through the coatings. Therefore, the anticorrosion properties of the composite coatings were improved by adding 0.2 wt% graphene, compared

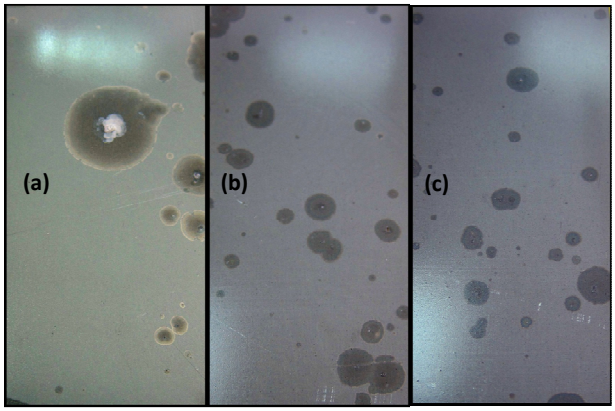

Fig. 7 Images of coated EG samples subject to the salt spray test after 48h (a) neat PU coating; (b) PTG-0.2 coating; (c) PTG-0.4 coating.

to neat PU coatings. When the graphene content reached 0.4 wt%, the graphene layers were self-aligned parallel to the substrate surfaces, which fully utilized the high surface area of graphene to interact with the electrolyte and prevent the electrolyte from penetration. Superior anticorrosion properties were testified by EIS analysis that under-painting corrosion didn't occur after 96h immersion in electrolyte.

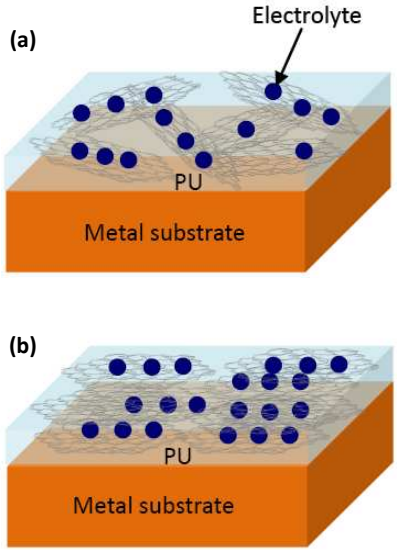

Fig. 8 Schematics of TGO/PU coatings (a) with randomly distributed TGO, which sealed up some area in the coating and gave lower absorption of electrolyte, and (b) with aligned TGO, which fully utilized the surface area of TGO as the barrier of electrolyte.

Acknowledgements

The authors gratefully acknowledge financial support from NSFC (U1260104, 51102170, 51102168, 51272157, 51102167), China.

References

1 D. Prasai, J. C. Tuberquia, R. R. Harl, G. K. Jennings and K. I. Bolotin, ACS Nano, 2012, 6, 1102-1108.
2 M. Schriver, W. Regan, W. J. Gannett, A. M. Zaniewski, M. F. Crommie and A. Zettl, ACS Nano, 2013, 7, 5763-5768.
3 C. H. Chang, T. C. Huang, C. W. Peng, T. C. Yeh, H. I. Lu, W. I. Hung, C. J. Weng, T. I. Yang and J. M. Yeh, Carbon, 2012, 50, 5044-5051.
4 Y. H. Yu, Y. Y. Lin, C. H. Lin, C. C. Chana and Y. C. Huang, Polym. Chem., 2014, 5, 535-550.
5 O. C. Compton, S. Kim, C. Pierre, J. M. Torkelson and S. T. Nguyen, Adv. Mater., 2010, 22, 4759-4763.
6 Y. H. Yang, L. Bolling, M. A. Priolo and J. C. Grunlan, Adv. Mater., 2013, 25, 503-508.
7 H. Kim, Y. Miura and C. W. Macosko, Chem. Mater., 2010, 22, 3441-3450.
8 N. Yousefi, M. M. Gudarzi, Q. B. Zheng, X. Y. Lin, X. Shen, J. J. Jia, F. Sharif and J. K. Kim, Composites Part A, 2013, 49, 42-50.
9 J. M. Yeh, S. J. Liou, C. Y. Lai and P. C. Wu, Chem. Mater., 2001, 13, 1131-1136.
10 C. S. Lu and Y. W. Mai, Phys. Rev. Lett., 2005, 95, 088303.
11 H. Kim, A. A. Abdala and C. W. Macosko, Macromolecules, 2010, 43, 6515-6530.
12 D. Y. Cai and M. Song, J. Mater. Chem., 2010, 20, 7906-7915.
13 J. Li, Z. Z. Yang, H. X. Qiu, Y. G. Dai, Q. B. Zheng, G. P. Zheng and J. H. Yang, J. Mater. Chem. A, 2013, 1, 11451-11456.
14 Q. B. Zheng, W. H. Ip, X. Y. Lin, N. Yousefi, K. K. Yeung, Z. G. Li and J. K. Kim, ACS Nano, 2011, 5, 6039-6051.
15 R. H. Alonso, L. Estevez, H. Q. Lian, A. Kelarakis and E. P. Giannelis, Polymer, 2009, 50, 2402-2410.
16 N. Yousefi, M. M. Gudarzi, Q. B. Zheng, S. H. Aboutalebi, F. Sharif and J. K. Kim, J. Mater. Chem., 2012, 22, 12709-12717.
17 S. Ansari, A. Kelarakis, L. Estevez and E. P. Giannelis, Small, 2010, 6, 205-209.
18 J. L. Baker, A. Widmer-Cooper, M. F. Toney, P. L. Geissler and A. P. Alivisatos, Nano Lett., 2010, 10, 195-201.
19 R. A. L. Jones, Soft Condensed Matter, Oxford University Press, New York, 2002, ch. 7, pp. 122.
20 I. Balberg, N. Binenbaum and N. Wagner, Phys. Rev. Lett., 1984, 52, 1465-1468.
21 Y. Zuo, R. Pang, W. Li, J. P. Xiong and Y. M. Tang, Corros. Sci., 2008, 50, 3322-3328.
22 A. Amirudin and D. Thieny. Prog. Org. Coat., 1995, 26, 1-28.
23 J. R. Scully, J. Electrochem. Soc., 1989, 136, 979-990.
24 R. Hirayama and S. Haruyama, Corrosion, 1991, 47, 952-958.
25 X. P. Liu, T. L. Zheng and J. P. Xiong, Int. J. Electrochem. Sci., 2013, 8, 11588-11595.
26 J. G. Liu, G. P. Gong and C. W. Yan, Electrochim. Acta, 2005, 50, 3320-3332.
27 X. W. Liu, J. P. Xiong, Y. W. Lv and Y. Zuo, Prog. Org. Coat., 2009, 64, 497-503.
28 J. J. Yoo, K. Balakrishnan, J. S. Huang, V. Meunier, B. G. Sumpter, A. Srivastava, M. Conway, A. L. M. Reddy, J. Yu, R. Vajtai and P. M. Ajayan, Nano Lett., 2011, 11, 1423-1427.
29 I. H. Tseng, Y. F. Liao, J. C. Chiang and M. H. Tsai, Mater. Chem. Phys., 2012, 136, 247-253.